Brittle-to-Ductile Transition in Uniaxial Compression of Silicon Pillars at Room Temperature

By *Fredrik Östlund, Karolina Rzepiejewska-Malyska, Klaus Leifer, Lucas M. Hale, Yuye Tang, Roberto Ballarini, William W. Gerberich,* and *Johann Michler**

Robust nanostructures for future devices will depend increasingly on their reliability. While great strides have been achieved for precisely evaluating electronic, magnetic, photonic, elasticity and strength properties, the same levels for fracture resistance have been lacking. Additionally, one of the self-limiting features of materials by computational design is the knowledge that the atomistic potential is an appropriate one. A key property in establishing both of these goals is an experimentally-determined effective surface energy or the work per unit fracture area. The difficulty with this property, which depends on extended defects such as dislocations, is measuring it accurately at the sub-micrometer scale. In this Full Paper the discovery of an interesting size effect in compression tests on silicon pillars with sub-micrometer diameters is presented: in uniaxial compression tests, pillars having a diameter exceeding a critical value develop cracks, whereas smaller pillars show ductility comparable to that of metals. The critical diameter is between 310 and 400 nm. To explain this transition a model based on dislocation shielding is proposed. For the first time, a quantitative method for evaluating the fracture toughness of such nanostructures is developed. This leads to the ability to propose plausible mechanisms for dislocation-mediated fracture behavior in such small volumes.

1. Introduction

The unprecedented growth in processing novel advanced materials has produced a commensurate need for measuring their properties. Clearly, any number of breakthroughs in measuring electronic, optical, magnetic, and mechanical properties of novel structures which depend upon chemistry and point defect distributions have occurred.[1–8] For example, modeling of optical responses can be assisted by 3D finite element models[4] and the effect of ultra-high pressures on hardness have been examined by diamond-anvil and quantum chemical simulations.[6] There have been fewer recent advances in measuring property data, but of note are those involving nanoforce-sensor developments at the atomic scale[7] and the plasticity of nanowires in tension.[8] Applications of first-principle, density-functional or multi-scale modeling methods have been applied to plasticity properties but with limited success due to the difficulties associated with extended defects.

For that reason, among others, one of the holy grails of the materials science and ceramics communities has remained elusive. A half century ago, researchers at U.C. Berkeley predicted the era of advanced ceramic materials, meaning ductile ceramics, was on the verge of realization.[9,10] This was mostly based upon direct imaging of dislocation structures in ceramic crystals such as MgO and the alkali halides associated with their plastic deformation at room temperature. However, bulk plasticity was never realized due to the inherent defect distributions in large volume ceramic structures. Modest improvements were achieved utilizing metastable structures such as partially stabilized zirconia.[11,12] Significant, ductile ceramics, however, require dislocation plasticity at room temperature.

There have been a number of recent nanoindentation-type or microelectromechanical systems studies of such plasticity in films, nanopillars, and nanowires.[13–15] Nevertheless, there have been fewer studies dealing with the fracture properties of relatively brittle, stand-alone, small volumes. While there have been a few semi-quantitative studies of nanospheres,[16] nanowires,[17] and nanopillars,[18] there has been no coupled, property measurements

[*] Dr. J. Michler, F. Östlund, K. Rzepiejewska-Malyska
Laboratory for Mechanics of Materials and Nanostructures
Empa - Materials Science & Technology
Feuerwerkstr. 39, CH-3602 Thun (Switzerland)
E-mail: johann.michler@empa.ch
Prof. K. Leifer
Electron Microscopy and Nanoengineering
Department of Engineering Sciences
Ångströmlaboratoriet, Lägerhyddsv. 1
751 21 Uppsala (Sweden)
L. M Hale, Prof. W. W Gerberich
Chemical Engineering and Materials Science
University of Minnesota, 151 Amundson Hall
Minneapolis, MN 55455
Dr. Y. Tang, Prof. R. Ballarini
Civil Engineering
University of Minnesota
Minneapolis, MN 55455

DOI: 10.1002/adfm.200900418

backed up by quantitative analysis of a scale dependent brittle-ductile transition in ceramics or semi-conductors except perhaps one.[19] In the present paper, it is proposed that the brittle-ductile transition is scale dependent, can be dropped hundreds of degrees centigrade and can be quantified in nanovolumes. Using single crystal silicon as a prototypical brittle material with a brittle-to-ductile transition temperature (BDT) of 550 °C in bulk form,[20] nanopillars as the small volume structures and finite element modeling of the experimentally developed cracks by in situ nanoindentation, the promise of ductile ceramics is explored.

2. Brittle-to-Ductile Transistion

In this study pillars with diameters ranging from 230–940 nm were prepared by a focused ion beam (FIB) technique. These were evaluated in compression using two instruments as described in the experimental section. Figure 1 shows the stress at which the pillars start deforming in a predominantly non-elastic manner as a function of the pillar diameter. For pillars deforming plastically this is the yield stress and for pillars cracking, it is the fracture strength. The results from the in situ compression experiments are in agreement with the results from the ex situ experiments, despite the fact that the former tended to bend. The average yield stress for the pillars that deformed plastically was 5.3 GPa with a standard deviation of 1.2 GPa. The brittle-to-ductile transition occurs between 310 and 400 nm. Under high hydrostatic pressures silicon can deform through phase transformation. The lowest pressure phase is called β-Sn and occurs at pressures above 11 GPa.[1] It is unlikely that the pressure at the middle of the pillars reaches this level since the yield stress is about a factor of two lower than this. Therefore the deformation has been mediated by dislocations.

There is a caution that should be noted considering a previous study of FIB-machined molybdenum-alloy single crystals.[21] In that study it was found that the gallium beam degraded the yield strength of the pillars from about 9.2 GPa to about 0.9 GPa. Given that the average yield strength for Si here was 5.3 GPa and using the commonly used ratio of 3 for converting to hardness, this gives 15.9 GPa. As this is slightly greater than the reported 14.2 GPa for nanohardness of silicon free of FIB machining,[22] it appeared that the FIB machining had little effect on silicon. Additionally, the average yield strength normalized on modulus for silicon gives a nearly identical value of 0.032 versus 0.029 for the molybdenum alloy of the FIB study[21] which was not subject to FIB milling (9.2 GPa / 320 GPa). This is probably due to the relatively small influence of low melting point liquid or solid metal films on covalent or ionic bonded solids compared to metals and their alloys. Still one should be aware of potential surface damage which may affect the frequency of dislocation nucleation sites after yielding commences. As most of the crack front is in the interior, this should not greatly affect the fracture result since the yield strength does not seem to be compromised.

Over the size range of 1 μm down to 200 nm the columns transitioned from predominantly brittle to ductile behavior at room temperature. This relatively sharp transition in scale in the 310 to 400 nm regime is reminiscent of the extremely sharp BDT found originally by St. John at 550 °C in bulk silicon.[20] It is astounding how much that transition temperature changes as the nanometer scale is approached. At slightly above room temperature, Nakao[13] had demonstrated in 4 μm thick pre-cracked samples under tension, a modest fracture toughness increase from 1.4 to 2.4 MPa $m^{1/2}$. Here, at an order of magnitude smaller length scale near 400 nm, the BDT at room temperature is uniquely featured by cracking versus no cracking at all. This is illustrated by the example columns in Figure 2 and 3 with the largest column having a crack length of 1120 nm in 2c, the medium size having a crack length of 250 nm in 3a and the smallest having no crack in 3b.

The results presented in this communication are not the first of compression tests on silicon pillars. A similar study was done by Moser, et al.,[18] but in this case the diameters of the pillars were 800 nm and larger. As a result, the transition from brittle to ductile behavior was not observed.[18] In addition three-point bending experiments on silicon beams with a thickness down to 255 nm[17] and two-point bending experiments on grown silicon nanowires with diameters between 200 and 300 nm[23] have shown no traces of plasticity. Bending experiments, however, differ from compression experiments in the aspect that in bending a part of the sample is subjected to tensile stresses. In another study indentation experiments were performed on silicon ridges with submicrometer widths.[24] In this case deformation by dislocations, in contrast to phase transformation, was observed. This was

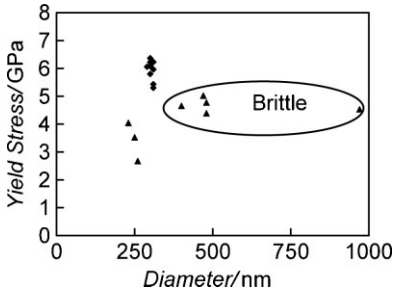

Figure 1. The critical engineering stress at which the pillars of varying diameters deviated from elastic behavior. The pillars that showed cracking are encircled; all the other pillars deformed purely plastic. The deformation behavior was determined by scanning electron microscopy and the engineering stress was calculated by taking the diameter at half the height of the pillar. The triangles correspond to experiments with an MTS and the diamonds correspond to experiments in situ.

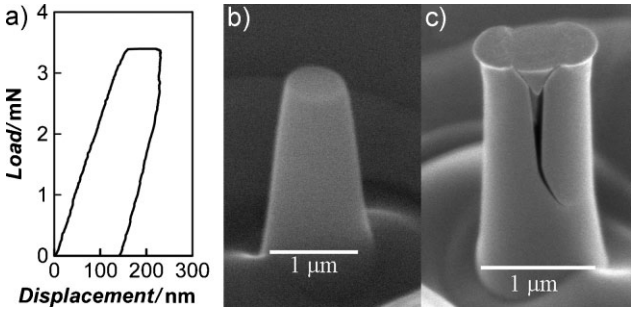

Figure 2. A compressed silicon pillar with 940 nm diameter at half the height of the pillar. The compression speed was 5 nm/s. (a) shows the load displacement curve for the compression. (b) shows the pillar before compression at a 55° angle. The tapering angle is 5° and the height of the pillar is 2.2 μm. (c) shows the pillar after compression at a 45° tilt in a high resolution SEM.

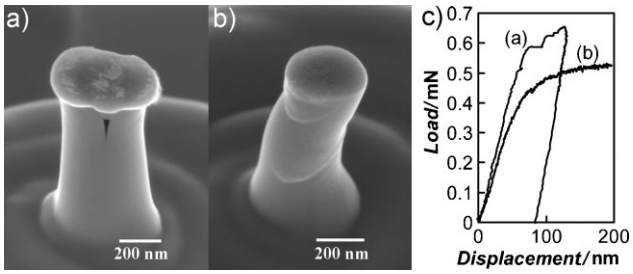

Figure 3. (a) and (b) shows HR-SEM images of two compressed silicon pillars at 45° tilt. The diameter of the pillars were 400 and 310 nm respectively. (a) was compressed with the MTS and (b) with the in situ setup. (c) shows load curves for the compression tests.

attributed to high shear stresses at the surface of the ridge allowing for dislocation nucleation at the surface. This allows the stress to be relaxed before the phase transformation occurs.

A study similar to the current one had previously been performed on gallium arsenide pillars.[25] In that study, pillars of 1 μm diameter were deformed plastically through uniaxial compression. Gallium arsenide is, like silicon, normally brittle and has a zinc-blende crystal structure, which is very similar to the diamond structure of silicon. The yield stress was 1.8 GPa, which is considerably lower than for silicon. The study on gallium arsenide was lacking tests on larger pillars; therefore the critical diameter was not pinpointed. Nonetheless, it showed that the critical diameter for gallium arsenide exceeds that of silicon by at least a factor of two.

In order to understand why smaller silicon pillars deform plastically it is important to understand how dislocations behave in silicon. Dislocations nucleate on the surface of the pillar and they move through the pillar on {111} planes. For a sample to be ductile, dislocations have to be generated at a sufficient rate and they have to be sufficiently mobile otherwise the pillar cannot accommodate the imposed deformation plastically and will fail through brittle fracture. Dislocations in silicon are generally dissociated into two partial dislocations that are separated by a stacking fault.[26] The dissociation distance depends on the applied stress and the mobilities of the two partial dislocations. If the width of a {111} plane crossing the pillar is smaller than the dissociation distance of the partials a single partial can nucleate on the side of the pillar and traverse the whole pillar without nucleating a trailing partial. This allows the pillar to deform solely through the nucleation and migration of single partials. If on the other hand, the width of the {111} plane exceeds the dissociation width of the partials the trailing partial has to nucleate. The mobilities of the two partials differ from each other.[26] The deformation rate for smaller pillars is limited by the mobility of the partial dislocation with the lowest activation energy since this will be the only occurring partial. For larger pillars the rate is limited by the mobility of the slower trailing partial. We propose that this is one possible mechanism for the observed brittle-to-ductile transition.

A second possibility is that dislocations in the shuffle set may be nucleated at very high stress in these small volumes. According to Pizzagalli, et al.,[27] the core configuration belonging to the shuffle set planes is favored for dislocation plasticity at low temperatures. For the shuffle set with widely spaced atoms, the bond breakage occurs on the {111} plane with atoms of the same index as opposed to the glide set for the same {111}. Here, breaks between much closer atoms of different indices break. These are favored at higher temperatures with partial dislocations. This shuffle set has been proposed to be the dominant plasticity mechanism at low temperatures based upon experimental work[28,29] and atomistic simulations.[27] Based upon a molecular dynamics study of unstable stacking faults in silicon, de Koning, et al.[30] had earlier suggested that the transition from the glide set to the shuffle set might be related to the brittle to ductile transition. They also demonstrated a strong pressure dependence and a large spread in the unstable stacking free energies, γ_{us}. The shuffle set had much lower energies and the spread between the two increased at lower temperatures.

From Sun and Beltz,[31] the effective stress intensity for dislocation nucleation under shear is given by

$$K_\tau = \eta\sqrt{\gamma_{us}\rho(\theta,\phi)} \tag{1}$$

where $\rho(\theta,\phi)$ for a specific crystal orientation is an inverse function of a given compliance matrix, $\Lambda_{\alpha\beta\Delta}$. With $\eta \sim$ unity,[31] one finds with the theoretical γ_{us} that the values of K_τ are somewhat smaller than the Griffith fracture value for the shuffle set dislocations. Similarly, along with the unstable stacking fault energy results determined by finite temperature dynamics modeling of silicon,[30] one also finds a stress intensity value for dislocation nucleation to be about 30 percent smaller under zero pressure at room temperature in the shuffle set compared to the glide set. Altogether, this might explain why the undissociated dislocations that were observed after a Vickers indentation at 77 K were of the shuffle set rather than the dissociated dislocations of the glide set.[32] It is proposed that one of these two mechanisms controls near room temperature in these small volumes.

To quantify the magnitude and character of the brittle-to-ductile transition, an elastic finite element analysis solution of a right cylinder column with a crack vertically aligned on a {110} plane was conducted. As described in the experimental/theoretical methods section, an isotropic elasticity solution was conducted to allow this method to be used for general crystalline materials, single crystal or polycrystalline, realizing that some deviations would result for highly anisotropic systems. For the two pillars exhibiting cracks in Figures 2c and 3a, simulations were conducted of the arrest stress intensity factor which is taken here as K_{IC}, the fracture toughness. The K_{IC} value along the crack profile was shown to be nearly constant for these two cases considering the crack front reached a circular arc with the best-fit position from the surface to the interior. Finite element simulations were carried out using ABAQUS with finite deformation.[33] Due to symmetry, a quarter of the pillar is built for both small and large specimens with diameter 400 nm and 940 nm, length (l) 800 nm and 2200 nm and tapering angle (θ) 5°. See Figure 4 with further explanation in the following section.

A summary of the findings in Figure 5 demonstrates that by reducing the pillar diameter by more than a factor of two that the K_{IC} more than doubles representing a work per unit fracture area or strain energy release rate (G_{IC}) increase of a factor of five since $G_{IC} \propto K_{IC}^2$. As thoroughly discussed in the methods section, this is a plastic energy dissipation mediated process and with the large

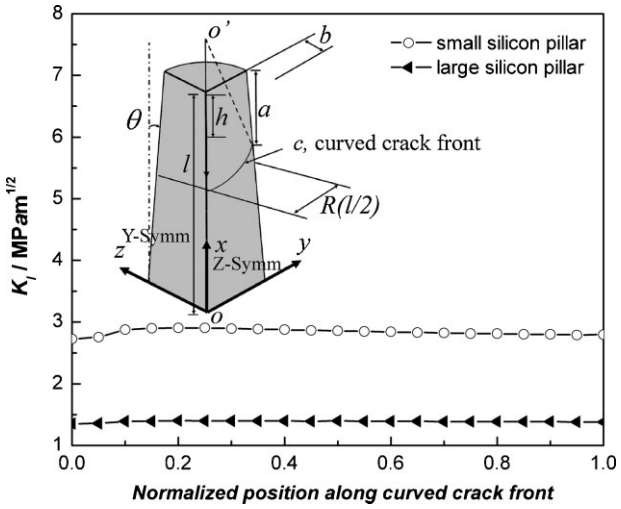

Figure 4. Finite element results of stress intensity factors along the arrested crack fronts shown for the silicon pillars of Figures 2c and 3a.

scale plasticity for the 300 nm versus the 400 nm (20 percent plastic strain versus 1 percent), the fracture toughness is proposed to be very large.

Returning to the question of dislocation mediated plasticity, there are two possible modes for movement of dislocations in silicon. They can move on either the widely separated shuffle sets or on the closer glide sets.[23] The actual mode of deformation is a debated topic that has not yet been fully resolved. At lower temperatures higher stresses can be reached before deformation occurs and this promotes the formation of shuffle dislocations. However, shuffle dislocations cannot dissociate into partial dislocations. This means that in order for either of the models described above to be correct, the dislocations have to be in the glide or shuffle set. To confirm this, a thorough transmission electron microscopy investigation is needed.

In summary, the nanoscopic compression experiments presented in this paper show, for the first time, that silicon can deform plastically in a uniaxial configuration at room temperature provided that the sample dimensions do not exceed a critical size. Sizes smaller than critical, on the order of 300 nm, experience a rapid rise in the fracture toughness.

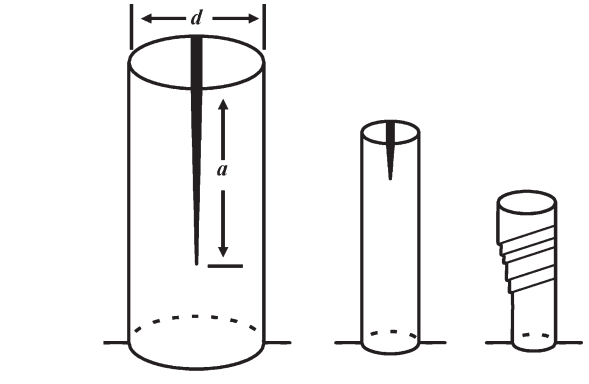

d [nm] =	940	400	300
a [nm] =	1250	25	0
K_{IC} [MPa m$^{1/2}$] =	1.3	2.9	>>3

Figure 5. Schematic of columns tested in Figures 2 and 3 with column and crack dimensions along with calculated fracture toughness values using FEM.

3. Experimental

This experimental/simulation/analytical section shows the detailed methods used in the experiments, the finite element solution for the fracture toughness calculations and the proposed mechanism for dislocation mediated toughness improvements. The micropillars were manufactured on a boron-doped silicon wafer ($\rho = 1$–$10\,\Omega$cm) by focused ion beam machining using a Lyra/XMU Dual beam from Tescan. The diameter was varied from 230 nm to 940 nm and the height was close to four times the diameter for all the pillars. The orientation of the wafer, and therefore also the symmetry axis of the pillars, was ⟨100⟩. In this configuration slip along four different {111} planes is equally favored. The energy of the gallium ions of the focused ion beam was 30 kV. Aside from the desired sputtering of a target, these ions cause damage to the surface. For silicon the main damage consists of an amorphous layer with a thickness of about 10 nm [34]. Furthermore, a focused ion beam cannot produce perfectly vertical structures; hence the pillars had a slightly conical shape. The tapering angle ranged between 2° and 6°.

Pillar Compression: The compression experiments were performed with two different setups: an MTS XP nanoindenter equipped with a diamond flat punch tip and a custom built indenter for usage within the chamber of a Hitachi S-4800 high resolution scanning electron microscope [35]. This in situ indenter allows the compression tests to be observed in real time in the scanning electron microscope. This provides valuable information about the deformation behavior and about the alignment of the tip and pillars. However, the maximum allowable load of the in situ indenter prohibited deformation of the larger pillars. Therefore, the ex situ setup was used for compressing these. Based on the initial deformation behavior the pillars could be divided into two disjoint sets: pillars deforming purely plastically and pillars that developed cracks in addition to a plastic deformation. The pillars with a diameter less than 310 nm belong to the first class and the pillars with diameters exceeding 400 nm to the second. Figures 2 and 3 show scanning electron microscope images and corresponding load-displacement curves from one pillar from each class.

Due to the absence of imaging data from the compressions with the ex situ setup each test was manually stopped as soon as the load-displacement curve deviated from elastic. A total of 8 successful compression tests were performed with this setup. Of these, 5 pillars had diameters exceeding 400 nm. All of these developed a vertical crack in the central part of the pillars during the compression. An example is shown in Figure 2. The crack presumably propagated on a {110} plane and it is interesting to note that it changes direction further down the pillar into what presumably is a {111} plane, the preferred cleavage plane of silicon. On the top of the pillar a wedge has been formed, driving the crack by separating the two halves of the pillar. The three remaining pillars that were compressed with the ex situ setup had diameters of 260 nm and below. All of these deformed purely plastically. The deformation was limited to the top of the pillars. The reason for this is that the diameter of the pillars are smallest at the top, hence the stress is highest.

Given that all pillars exhibited plastic deformation, it is important to define what is meant by a brittle-to-ductile transition. The tops of the pillars are rounded and in contact giving rise to larger local stresses, plastic deformation and potential nucleation of cracks at the top. Originally, following the Rice-Thompson paper of 1974 [36], many adhered to the either/or proposition that a crack would either emit dislocations and cause blunting or undergo brittle cleavage, particularly in single crystals. However, many experimental and theoretical studies demonstrated that cleavage could be accompanied by substantial amounts of dislocation plasticity [37–40]. As a result, one can view the BDT as a small amount of plasticity accompanying cleavage at low temperatures changing to larger

amounts of plasticity accompanying cleavage or other fracture modes at higher temperature resulting in an increase in the fracture toughness. Depending on both dislocation nucleation and kinetics, this can be either a slowly varying transition [41], or an abrupt one [20] with test temperature. In the present case, the critical variable for the transition is size scale not temperature.

Using the in situ setup 11 more pillars with diameters from 290 nm to 310 nm were compressed. These pillars were compressed to larger strains than the pillars compressed with the ex situ setup. During the compression tests videos were recorded with the scanning electron microscope. These revealed that all the pillars, in addition to deforming plastically, were bent slightly sideways. This behavior is probably a result of imperfect alignment between the indenter tip and the pillars. The bending results in an uneven stress distribution, which shows up in the post-deformation images as a tilted top. This effect was not observed for the pillars compressed in the ex situ setup suggesting that the pillars were perfectly aligned. As the pillars were deformed to higher strains they developed slip bands indicating slip on {111} planes. The amount of deformation the pillars were able to accommodate was astonishing; in the example of Figure 3b the engineering strain reached 22 percent. It should be noted that for pillar compression experiments there is a hydrostatic pressure just under the tip, arising from the friction between the tip and the pillar, and at the bottom of the pillar arising from the confining effect of the substrate. A simple finite element method simulation showed that this pressure does not extend into the central parts of the pillars. A simulated compression experiment of a silicon pillar with 500 nm diameter, 2 μm height and 2° tapering angle, using a flat, rigid tip and a friction coefficient of 0.11 [42] showed that in more than 60 percent of the length of the pillar the radial stress is lower than one percent of the stress in the axial direction when the engineering stress is 5 GPa.

Fracture Toughness Analysis: Regarding the fracture toughness measurements, an initial estimate was made from Broeks' analysis [43] of a wedge opening displacement of a crack in a plate. This assumed a thru-crack of length, a, in a beam of thickness, $2R$, with a wedge opening of $2b$. The analytical solution, given by

$$K_{IC} = \frac{\sqrt{3}EbR^{3/2}}{4a^2(1 - \nu^2)} \tag{2}$$

used the modulus, $E = 160$ GPa, Poisson's ratio, $\nu = 0.218$, and the sample dimensions of Figure 5 with the diameter, $d = 2R$. For the two pillars that cracked, the half-wedge openings were measured to be 30 nm and 15 nm for the larger and smaller diameters, respectively. Using the beam thickness as the pillar diameter gave calculated K_{IC} values of 0.9 and 3.5 MPa $m^{1/2}$ for the large and small pillars. These gave values similar to those reported in Figure 5 for the numerical analysis. However, due to the inapplicability of the analytical solution which considered a straight-thru crack in a rectangular section, as opposed to a curved crack front in a right cylinder, the following numerical solution was employed.

The crack front is assumed to be an arc with radius c and its center is located on the axis of the pillar (Figure 4). The crack lengths at the surface are measured from experimental results, 250 nm and 1250 nm for small and large pillars, respectively. The bottom of the finite element method model is fixed and the silicon sandwiched between the crack surfaces (Figure 3) is treated as a wedge with length h and half thickness b, which are 150 nm and 10 nm for the pillar with small diameter (300 nm and 30 nm for the larger one). The inserted wedge is modeled implicitly: a constant displacement b is applied at the top region of the crack seam (depth h to the top of the pillar). During the simulation, the J-integral is calculated, and then the stress intensity factor, K_I, along the crack front is evaluated through

$$K_I(x, y) = \sqrt{\frac{E}{1 - \nu^2} J(x, y)} \tag{3}$$

For any radius c given initially, K_I is a function of the position of the crack front. However, the fracture toughness should be a constant for the final crack profile in a homogeneous isotropic material. In order to obtain the fracture toughness, we iterate c until the standard deviation of the stress intensity along the crack front reaches the minimum. Hence, the mean value of K_I will approach the fracture toughness. The resulting radius, c, of the curved crack equals 640 nm for the small pillar and 1410 nm for the large pillar. K_I for both pillars are shown in Figure 4, which appear almost constant after iteration. Therefore, the averaged stress intensity factor, K_I, along the crack front is the fracture toughness, K_{IC}, and is found to be ~1.3 MPa $m^{1/2}$ and 2.9 MPa $m^{1/2}$ for the large and small diameter specimens respectively. There is one possible limitation to the experimental procedure due to the lack of flatness at the tops of the pillars. This caused slightly asymmetrical loading which could initially increase the Mode II of any nascent defects due to additional deviatoric stresses. However, as the deformation proceeded and crack-wedging commenced, this became fairly symmetrical in Figures 2 and 3. Also, as the wedging crack is dominated by Mode I cracking, the considerably smaller contributions from Mode II are not considered to be a major influence in the crack arrest condition calculated.

Given the proposed dislocation-mediated toughness increase, it is important to consider in detail how a relatively small number of dislocations in brittle materials of small dimension might achieve this. A recent collection of fracture toughness data for intermetallics, semiconductors, oxides, nitrides, carbides, and silicides demonstrated that a crack extension force concept could be used to predict fracture toughness [44]. The balancing force at crack arrest was interpreted in terms of shielding dislocations and the force on a dislocation. Except for the intermetallics, a simple fit based on $N = 12$ dislocations, could be used to predict the toughness of 15 brittle materials as evaluated by indentation into bulk single-crystals or relatively large-grained polycrystals. This was given by [44]

$$K_{IC} \approx \frac{4}{3}\left[\frac{N\mu\sigma_{ys}b}{1 - \nu}\right]^{1/2} \tag{4}$$

with $\mu\sigma_{ys}$ b the product of the shear modulus, yield strength and Burgers vector. Knowing that the yield strength of the larger column was less than or equal to 4.8 GPa, one could determine the minimum shielding number, N, from Eq. (4). Using the toughness of 1.3 MPa $m^{1/2}$ from Figure 5 for the 940 nm diameter column, this was found to be 10 dislocations, reasonably consistent with bulk behavior. For the 400 nm diameter column, however, with a yield strength of 5.7 GPa and a $K_{IC} = 2.9$ MPa $m^{1/2}$, 42 shielding dislocations are calculated. This is not so many dislocations considering that the pillar height would only have to deform inelastically about 1 percent. The fact that 20 percent plastic strains were achieved at only slightly smaller diameters attests to the sharp rise of this size-affected ductility transition. Clearly, there is adequate space in the column as this would represent an average dislocation spacing of about 13 nm for the 400 nm diameter pillar and multiple slip planes have been activated in the smaller pillar of Figure 3b. There are many limitations to this type of first-order assessment since all interaction forces have not been properly counted. Using discretized dislocation models for all of the stress interactions would include the stress due to dislocations interacting with each other, the stress due to the crack interacting with all dislocations, the interaction of the external stress and the crack with the external applied stress. Such calculations are possible [45] to confirm the blocked slip band model proposed here.

Acknowledgements

WWG would like to acknowledge support of the Air Force through an AOARD-08-4131 program dedicated to understanding plasticity and fracture in hard materials.

Received: February 9, 2009
Revised: May 11, 2009
Published online: June 18, 2009

[1] M. D. Uchic, D. M. Dimiduk, J. N. Florando, W. D. Nix, *Science.* **2004**, *305*, 986.
[2] C. Kim, W. Gu, M. Briceno, I. M. Robertson, H. Choi, K. Kim, *Adv. Mater.* **2008**, *20*, 1859.
[3] O. H. Park, J. Y. Cheng, M. W. Hart, T. Topuria, P. M. Rice, L. E. Krupp, R. D. Miller, H. Ito, H.-C. Kim, *Adv. Mater.* **2008**, *20*, 738.
[4] V. Myroshnychenko, E. Carbo/-Argibay, I. Pastoriza-Pantos, J. Perez-Juste, L. M. Liz-Marzan, F. J. Garcia de Abajo, *Adv. Mater.* **2008**, *20*, 4288.
[5] G. A. DeVries, F. R. Talley, R. P. Carney, F. Stellacci, *Adv. Mater.* **2008**, *20*, 4243.
[6] Q. Gu, G. Krauss, W. Steurer, *Adv. Mater.* **2008**, *20*, 3620.
[7] X. Han, Z. Zhang, Z. L. Wang, *NANO* **2007**, *2*, 249.
[8] X. Han, K. Zheng, Y. Zhang, X. Zhang, Z. Zhang, Z. L. Wang, *Adv. Mater.* **2007**, *19*, 2112.
[9] A. F. Gorum, E. R. Parker, J. A. Pask, *J. Am. Ceramic Soc.* **1958**, *41*, 161.
[10] E. R. Parker, *ASTM Spec. Tech. Publ*. Am. Soc. Test. Mater. Philadelphia, PA **1960**, 283, 52.
[11] R. C. Garvie, R. H. Hannink, R. T. Pascal, *Nature* **1975**, *258*, 703.
[12] M. V. Swain, R. H. J. Hannick, R. C. Garvie, *Fracture Mechanics of Ceramics*, vol. 6, R. C. Brandt, et al., ed, Plenum Press, NY **1983**, 339.
[13] S. Nakao, T. Ando, M. Shikida, K. Sato, *J. Micromech. and Microengng.* **2008**, *18*, 015026/1.
[14] X. D. Han, Y. F. Zhang, K. Zheng, X. N. Zhang, Y. Hao, X. Y. Guo, J. Yuan, Z. L. Wang, *Nanolett.* **2007**, *7*, 452.
[15] X. D. Li, B. Bhushan, *Surface and Coatings Technology* **2003**, *163–164*, 521.
[16] W. M. Mook, J. D. Nowak, C. R. Perrey, C. B. Carter, R. Mukherjee, S. L. Girshick, P. H. McMurry, W. W. Gerberich, *Phys. Rev. B.* **2007**, *75*, 214112/1.
[17] T. Namazu, Y. Isono, 0-7803-774-3103 *IEEE Trans* **2003**, 662.
[18] B. Moser, K. Wasmer, L. Barbieri, J. Michler, *J. Mater. Res.* **2007**, *22*, 1004.
[19] W. W. Gerberich, J. Michler, W. M. Mook, R. Ghisleni, D. D. Stauffer, R. Ballarini, *J. Mater. Res.* in press.
[20] C. St. John, *Phil. Mag.* **1975**, *32*, 1193.
[21] S. Shim, H. Bei, M. K. Miller, G. M. Pharr, E. P. George, *Acta Mater.* **2009**, *57*, 503.
[22] M. F. Doerner, D. S. Gardner, W. D. Nix, *J. Mater. Res.* **1986**, *1*, 845–851.
[23] S. Hoffmann, I. Utke, B. Moser, J. Michler, S. H. Christiansen, V. Schmidt, S. Senz, P. Werner, U. Gösele, C. Ballif, *Nanolett.* **2006**, *6*, 622.
[24] A. M. Minor, E. T. Lilleodden, M. Jin, E. A. Stach, D. C. Chrzan, J. W. Morris, Jr, *Phil. Mag.* **2005**, *85*, 323.
[25] J. Michler, K. Wasmer, S. Meier, F. Östlund, K. Leifer, *APL* **2007**, *90*, 043123/1.
[26] K. Wessel, H. Alexander, *Phil. Mag.* **1977**, *35*, 1523.
[27] L. Pizzagalli, P. Beauchamp, J. Rabier, *Europhys. Lett.* **2005**, *72*, 410.
[28] J. Rabier, J. L. Demenet, *Phys. Stat. Sol. (a)* **2005**, *202*, 944.
[29] J. Rabier, M. F. Denanot, J. L. Dermenet, P. Cordier, *Mater. Sci. Engng. A* **2004**, *387*, 124.
[30] M. de Koning, A. Antonelli, M. Bazant, E. Kaxiras, *Phys. Rev. B* **1998**, *58*, 12555/1.
[31] Y. Sun, G. E. Beltz, *J. Mech. Phys. Solids* **1994**, *42*, 1905.
[32] K. Asaoka, T. Umeda, S. Arai, H. Saka, *Mater. Sci. Engng. A* **2005**, *400*, 93.
[33] ABAQUS. *ABAQUS 6.6 user's manual*, ABAQUS Inc., Pawtucket, RI **2006**.
[34] S. Rubanov, P. R. Munroe, *J Micros.* **2004**, *214*, 213.
[35] K. A. Rzepiejewska-Malyska, G. Bürki, J. Michler, R. C. Major, E. Cyrankowski, S. A. F. Asif, O. L. Warren, *J. Mater. Res.* **2008**, *23*, 1973.
[36] J. R. Rice, R. Thomson, *Phil. Mag.* **1974**, *29*, 73.
[37] B. S. Mujumdar, S. J. Burns, *Acta metall.* **1981**, *29*, 579.
[38] M. J. Lii, X. F. Chen, Y. Katz, W. W. Gerberich, *Acta metall. mater.* **1990**, *38*, 2435.
[39] M. Ellis, *Ph.D. Thesis*, University of Oxford, UK **1991**, p. 50.
[40] H. Huang, W. W. Gerberich, *Acta metall. mater.* **1994**, *42*, 639.
[41] P. G. Marsh, W. W. Gerberich, *Acta metall. mater.* **1994**, *42*, 613.
[42] S. Niederberger, D. H. Gracias, K. Komvopoulos, G. A. Somorjai, *J. App. Phys.* **2000**, *87*, 3143.
[43] D. Broek, *Elementary Engineering Fracture Mechanics*, 4th ed., Kluwer Academic, London **1991**, p. 166.
[44] W. W. Gerberich, W. M. Mook, C. B. Carter, R. Ballarini, *Int. J. Fract.* **2007**, *148*, 109.
[45] H. Huang, W. W. Gerberich, *Acta metall. mater.* **1992**, *40*, 2873.